

Electronic energy levels in $\text{In}_x\text{Ga}_{1-x}\text{As}/\text{InP}$ strained-layer superlattices

D. Gershoni, J. M. Vandenberg, R. A. Hamm, H. Temkin, and M. B. Panish
AT&T Bell Laboratories, Murray Hill, New Jersey 07974

(Received 10 April 1987)

We use intentionally-lattice-mismatched superlattices of $\text{In}_x\text{Ga}_{1-x}\text{As}/\text{InP}$, where $0.3 < x < 0.8$, to study the energy levels of confined-particle states characteristic of strained-layer superlattices. We demonstrate that the energy difference between the lowest heavy- and light-hole exciton levels of $\text{In}_x\text{Ga}_{1-x}\text{As}$ quantum wells changes continuously with strain. For $x < 0.44$ the exciton levels switch positions so that the light hole becomes the lower-energy state. The experimental results can be modeled with very high accuracy over the entire range of In compositions studied with a phenomenological deformation-potential theory.

In recent years, much attention has been given to strained-layer superlattices (SLS's), in which multilayer structures are grown lattice mismatched to the substrate but with the layer thickness small enough to accommodate the mismatch strain coherently rather than by misfit dislocations. The elastic layer strain gives rise to a number of interesting properties and SLS's can be conveniently used to study strain effects. However, in a true SLS system the sign of strain is difficult to vary. In this work, we demonstrate the use of $\text{In}_x\text{Ga}_{1-x}\text{As}/\text{InP}$ SLS structures which can be either positively or negatively strained to explore the relationship between strain and electronic levels of quantum wells. This possibility has been discussed by People¹ and a study of strain effects has been carried out in the $\text{In}_x\text{Ga}_{1-x}\text{As}/\text{In}_x\text{Al}_{1-x}\text{As}$ system by Nishi, Hirose, and Mizutani.² In $\text{In}_x\text{Ga}_{1-x}\text{As}/\text{InP}$ the strain and quantum size effects can be independently controlled and a direct comparison to the nonstrained, lattice-matched system can be made. In this work, we use optical techniques to identify experimentally the energies of the electron-light-hole and electron-heavy-hole transitions as a function of compositional strain. The superlattice dimensions, as well as the strain, are measured by high-resolution x-ray diffraction. Excellent agreement is obtained between these experimental results and a deformation-potential model.

The $\text{In}_x\text{Ga}_{1-x}\text{As}/\text{InP}$ SLS samples used in this work have been grown by gas-source molecular-beam epitaxy (GSMBE). This technique is particularly well suited for growth of structures containing both As and P and allows for excellent control of the layer thicknesses, composition, and lattice match.³ The structures used in our experiments are described in the inset of Fig. 1. The samples were grown on a (100)-oriented InP substrate, on which a 0.25- μm -thick InP buffer layer was deposited prior to the superlattice. The superlattice region consisted of ten $\text{In}_x\text{Ga}_{1-x}\text{As}$ wells, with the thickness ranging from 75 to 100 Å in different samples, separated by 500-Å-thick InP barriers. The concentration of In in the five samples was varied from $x=0.3$ to 0.8, resulting in one lattice-matched sample (with $x=0.53$), two samples with lattice constant larger than that of the substrate, i.e., subjected to compressive biaxial stress, and the remaining two under tension.

Figure 1 presents the high-resolution Cu $K\alpha_1$ x-ray diffraction scans of the three samples with midrange In concentration x . The spectrum of the lattice-matched superlattice shows the presence of up to 11 orders of satellite reflections, indicative of the structural perfection of the sample. The satellite reflections show a highly symmetric intensity distribution on both sides of the (400) InP peak, as expected from strain-free layers. In comparison, the asymmetric shape of the top trace, with its enhanced

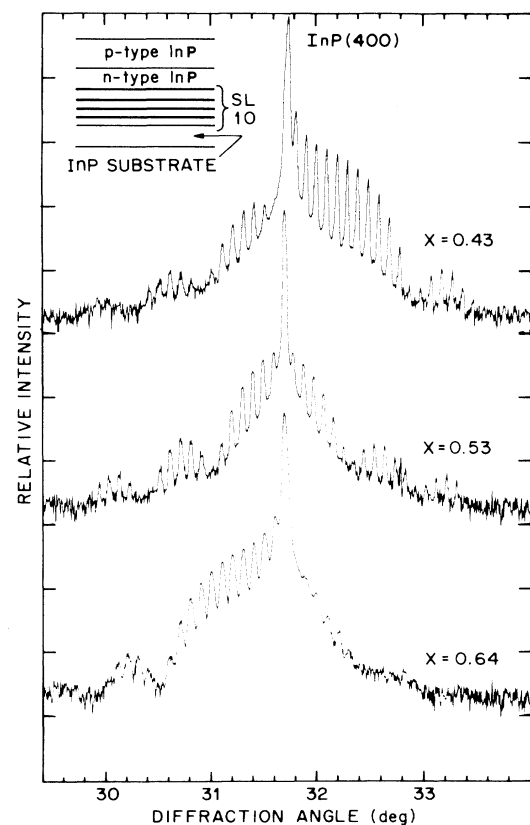


FIG. 1. X-ray diffraction scans of the lattice matched $x=0.53$, and strained $\text{In}_x\text{Ga}_{1-x}\text{As}/\text{InP}$ superlattices. Inset shows details of the structures.

right-hand-side diffraction intensity is indicative of an in-plane extension strain resulting in lattice compression in the growth direction, which is monitored by the (400) diffraction scan. The opposite sign of the strain results in the enhanced left side of the bottom trace. Despite the lattice mismatch, however, the strained samples retain their structural integrity, as judged by the sharpness and intensity of the satellite reflections. Using a kinematic step model previously described^{4,5} the x-ray scans can be computer simulated by fitting the lattice parameter of the well and the number of molecular layers in the well and the barrier. The well thickness and strain can be thus very accurately extracted, and the In concentration can be calculated using elastic theory and Vegard's law. The agreement between In concentration and SL dimensions extracted in this way and those estimated from the growth parameters is very good.

Figure 2 describes the low-temperature photoluminescence spectra of the SLS samples as a function of In concentration x . The spectral peaks shown are due to radiative recombination of the $1s$ exciton within the $\text{In}_x\text{Ga}_{1-x}\text{As}$ quantum wells. It is noteworthy that while x varies considerably from the lattice-matched composition and the exciton energy shifts by as much as 0.2 eV, corresponding to a wavelength shift of over 4000 Å, no significant degradation of the luminescence intensity is observed. This is consistent with the absence of nonradiative defects, such as misfit dislocations, in the strained samples. A slight broadening of the exciton peak was observed only in the two samples furthest away from the lattice-matched composition. This is attributed to the presence of a few monolayers of the quaternary In-Ga-As-P at the well to barrier interface.⁴ The excellent quality of the optical properties of these samples is maintained up to room temperature.

The polarized room-temperature photocurrent response spectra of rib-loaded waveguides prepared from our structures are used to discriminate between the heavy- and light-hole transitions. Two traces are presented in Fig. 3 for each of the samples studied. These spectra are ob-

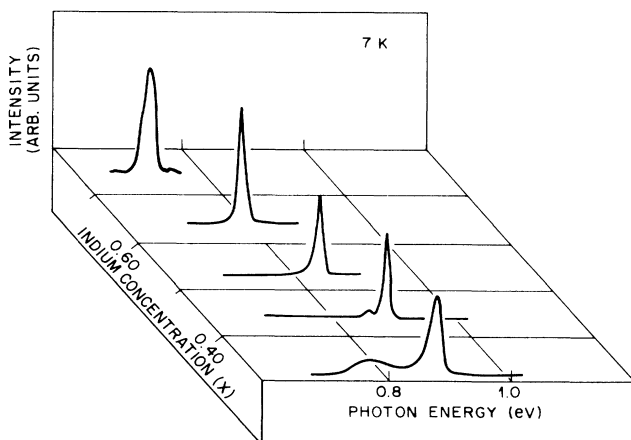


FIG. 2. Low-temperature photoluminescence spectra of $\text{In}_x\text{Ga}_{1-x}\text{As}$ superlattices as a function of In concentration.

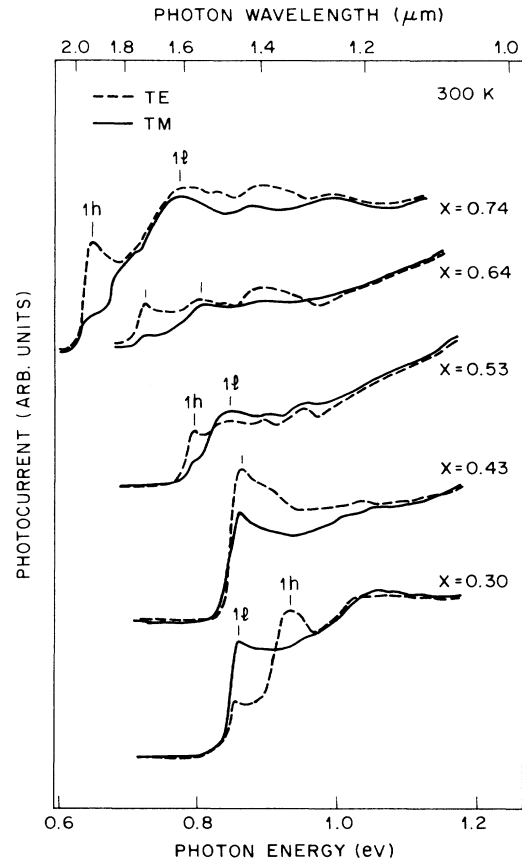


FIG. 3. Polarized room-temperature photocurrent spectra of strained-layer samples. Heavy and light excitonic transitions are indicated. The $1s$ exciton transition is forbidden in the TM polarization.

tained with the incident light polarized either parallel (TE polarization) or normal (TM polarization) to the superlattice layers. The heavy-hole transition is strictly forbidden in the TM polarization by the exciton selection rules.⁶ For these studies, the samples were prepared by photolithographically defining 80- μm -wide waveguide mesas cleaved to a length of 350 μm . A tungsten lamp dispersed with a grating spectrometer was used as an excitation source and light coupled through the cleaved facets into the waveguide formed by the superlattice by means of a 50 \times microscope objective. The resulting photocurrent spectra were detected using conventional lock-in techniques, digitized, and corrected for the systems response.

In each spectrum of Fig. 3 the heavy- and light-hole transitions can be readily identified by their polarization dependence and spectral shift. Considerable changes are observed in the energy difference of these two transitions as a function of In concentration. In samples with $x > 0.53$, the lattice-matched composition, the light-hole level is found, as expected, above the heavy-hole level, i.e., at higher energies. In the sample with $x = 0.43$ the energies of the two transitions, as detected by the polarized response spectra, are found to overlap. At even lower In concentration of $x = 0.30$ the exciton levels switch posi-

tions so that the light hole becomes the lower-energy state. A similar observation was reported by Schuber, Fritz, and Dawson⁷ who directly measured the light-hole masses in $\text{In}_{0.2}\text{Ga}_{0.8}\text{As}/\text{GaAs}$ SLS's and by Nishi *et al.*² who assigned the light-hole-electron transition to their lowest-energy transmission peaks. The energy levels of the $1s$ light- (filled circles) and heavy- (open circles) hole excitons deduced from the spectra of Fig. 3 are plotted in Fig. 4 vs In concentration. Also shown in Fig. 4 are the calculated energies of both the $1s$ light- and heavy-hole-electron transitions for 75-\AA -thick quantum wells.

Commensurate growth of strained $\text{In}_x\text{Ga}_{1-x}\text{As}$ on (100)-oriented InP substrate subjects these layers to a biaxial in-plane strain. The epitaxial layers experience a tetragonal distortion, resulting in a very simple form of the strain tensor e_{ij} . If we define $z\parallel[001]$ (i.e., along the growth direction) it follows that e_{ij} has only diagonal components with $e_{xx}=e_{yy}=e_{\parallel}$ and $e_{zz}=-2(C_{12}/C_{11})e_{\parallel}=e_{\perp}$,⁸ where e_{\parallel} (e_{\perp}) are the diagonal strain-tensor components parallel (perpendicular) to the growth plane and C_{ij} are the components of the elastic stiffness tensor.^{6,9} Knowing the elements of the strain tensor one can readily apply the phenomenological deformation-potential theory^{6,8,9} to calculate the effect of strain on the electronic states of the system under study. The calculation of the energy levels was carried out in the following way. First, commensurate growth was assumed, so that the in-plane lattice constant of the superlattice is always equal to that of the InP substrate and the in-plane strain components are given by $e_{\parallel}=[a_{\text{InP}}-a(x)]/a(x)$, where $a_{\text{InP}}=5.8688\text{ \AA}$ is the lattice constant of InP, $a(x)$ is the lattice constant of the relaxed $\text{In}_x\text{Ga}_{1-x}\text{As}$, and x is the In concentration as extracted from x-ray diffraction measurements. Lattice constants of various ternary compositions can be calculated from the known lattice constants of InAs and GaAs using Vegard's law.¹⁰ The same interpolation pro-

cedure was used to obtain all other material parameters of ternary alloys, such as the stiffness coefficient tensor $C_{ij}(x)$, the electron and light- and heavy-hole effective masses, the valence-band deformation potentials $a_v(x)$ and $b_v(x)$ (notation of Hensel and Feher⁶ and Bir and Pikus^{6,9}), and the energy-band-gap dependence on hydrostatic pressure $dE_g/dp(x)$.¹⁰ The band offsets were estimated in a similar way from the recently published synchrotron-radiation data for the parent binary compounds.¹¹ For the lattice-matched composition we calculate the valence-band offset ΔE_v to be equal to 59% of the total band-gap discontinuity, in agreement with the work of Forrest, Schmidt, Wilson, and Kaplan.¹² Finally, parabolic interpolation, which takes into account the bowing, was used to calculate the energy-gap dependence on the In concentration.¹³

With the calculated strain-tensor components, the difference between the strained and strain-free ternary band gap could be calculated according to

$$\Delta E_g(x) = [-dE_g(x)/dp] \times \left\{ \frac{1}{3} [C_{11}(x) + 2C_{12}(x)] \right\} [2e_{\parallel} + e_{\perp}], \quad (1)$$

where $\frac{1}{3}[C_{11}(x) + 2C_{12}(x)]$ is the bulk modulus of the ternary layer. The expressions in the square and curly brackets describe the hydrostatic deformation potential. The change in the valence-band offset with the hydrostatic part was calculated, similarly to Eq. (1), according to

$$\Delta E_v(x) = a_v(x)(2e_{\parallel} + e_{\perp}), \quad (2)$$

where $a_v(x)$ is the ternary valence-band hydrostatic deformation potential.¹⁰ The effects of hydrostatic strain on the conduction-band offset can be calculated simply by subtracting Eq. (2) from Eq. (1). The hydrostatic part of the strain changes the direct energy gap and, since the change is not equally distributed between the conduction

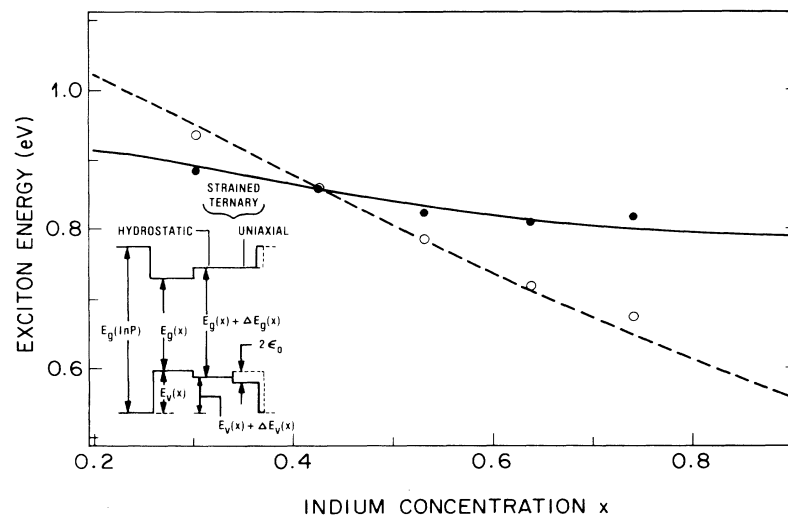


FIG. 4. Excitonic transition energies are plotted vs indium concentration (open and filled circles for heavy and light holes, respectively). Lines indicate calculated transition energies for 75-\AA -thick quantum wells. Data points for $x=0.3$ and 0.74 , obtained on 100-\AA -thick wells, were corrected for the appropriate quantum-size exciton shift. Inset shows band-gap changes with biaxial strain.

and valence bands, it directly influences the band-offset parameters. The uniaxial part of the strain results in removing the valence-band degeneracy at the Brillouin-zone center. This effect has been studied experimentally in the bulk GaAs (Ref. 14) and InAs,¹⁵ parent binary compounds of the ternary material. The valence-band splitting due to the uniaxial strain was calculated, according to

$$\varepsilon_0 = b_v(x)(e_{\perp} - e_{\parallel}) , \quad (3)$$

where ε_0 is half the energy splitting between the $(\frac{3}{2}, \frac{3}{2})$ and $(\frac{3}{2}, \frac{1}{2})$ valence-band sublevels and $b_v(x)$ is the ternary shear deformation potential for the [100] strain. These effects are illustrated schematically in the inset of Fig. 4. The quantum size effect, which like the uniaxial strain determines a preferred spatial direction (again the growth direction parallel to \mathbf{z}), also removes the valence-band degeneracy by creating the so-called heavy- and light-hole states.¹⁶ The two effects add in case of compressive strain and subtract in case of extensive strain. The quantum size effect was calculated for 75-Å wells using the resonance tunneling method¹⁷ for electrons and heavy and light holes separately. The resulting transition energies of the light (solid line) and heavy (dashed line) holes are plotted as a function of composition in Fig. 4. The strain-induced mixing between the spin-orbit split-off

band and the $(\frac{3}{2}, \frac{1}{2})$ valence band was neglected because of the relatively large spin-orbit splitting in this material.¹⁰ Similarly, the exciton binding energy which amounts to a few meV,¹⁷ was also neglected. Despite that, the agreement with the experimental data is quite satisfactory, as demonstrated in Fig. 4. This is especially so in view of the fact that the material parameters are interpolated from the binary values and not measured directly. It should be noted that the energy of the 1s exciton is not very sensitive to the conduction-to-valence-band offset ratio. A systematic 15% variation in the valence-band offset did not cause any appreciable change in the calculated curves. The higher-order excitons are expected to be more sensitive to that parameter. On the other hand, in order to obtain the agreement shown in Fig. 4, one must conclude that most of the band-gap changes induced by variation in the In concentration occur in the conduction-band offset.

In summary, we have used $\text{In}_x\text{Ga}_{1-x}\text{As}/\text{InP}$ superlattices with $0.3 < x < 0.8$ to study the effects of strain on the electronic properties of strained-layer superlattices. We show that the quantum-size effects, and in particular the energy difference between the heavy- and light-hole transitions, can be used to monitor the superlattice strain. The experimental data can be described very accurately by a simple phenomenological deformation potential theory.

¹R. People, Appl. Phys. Lett. **50**, 1604 (1987).

²K. Nishi, K. Hirose, and T. Mizatani, Appl. Phys. Lett. **49**, 194 (1986).

³M. B. Panish, Prog. Cryst. Growth Charact. **12**, 1 (1986).

⁴J. M. Vandenberg, S. N. G. Chu, R. A. Hamm, M. B. Panish, and H. Temkin, Appl. Phys. Lett. **49**, 1302 (1986).

⁵J. M. Vandenberg, R. A. Hamm, M. B. Panish, and H. Temkin, J. Appl. Phys. (to be published).

⁶J. C. Hensel and G. Feher, Phys. Rev. **129**, 1401 (1963).

⁷J. E. Schuber, I. J. Fritz, and L. R. Dawson, Appl. Phys. Lett. **46**, 182 (1985).

⁸G. C. Osbourn, Mater. Res. Soc. Symp. Proc. **25**, 455 (1984).

⁹G. L. Bir and G. E. Pikus, *Symmetry and Strain Induced Effects in Semiconductors* (Halsted, New York, 1974).

¹⁰S. Adachi, J. Appl. Phys. **53**, 8775 (1982).

¹¹R. S. Bauer and G. Margaritondo, Phys. Today **40** (No. 13),

34 (1987).

¹²S. R. Forrest, P. H. Schmidt, R. B. Wilson, and M. L. Kaplan, Appl. Phys. Lett. **45**, 1199 (1984).

¹³Ref. 10, formula (9b) gives a bowing parameter which agrees with the bulk band gap of $\text{In}_{0.53}\text{Ga}_{0.47}\text{As}$ measured in our samples.

¹⁴M. Chandrasekhar and F. H. Pollack, Phys. Rev. B **15**, 2127 (1977).

¹⁵P. Y. Yu, M. Cardona, and F. H. Pollack, Phys. Rev. B **3**, 340 (1971).

¹⁶G. Bastard and J. B. Brum, IEEE J. Quant. Electron. **22**, 1625 (1986).

¹⁷D. A. B. Miller, D. S. Chemla, T. C. Damen, A. C. Gossard, W. Wiegman, T. H. Wood, and C. A. Burrus, Phys. Rev. B **32**, 1043 (1985).